Facile Synthesis of Silica-Polymer Monoliths Using Nonionic Triblock Copolymer Surfactant for Efficient Removal of Radioactive Pollutants from Contaminated Seawater

Nada Abdelmageed[a], Waleed El-Said [b,c], Ahmed Younes [a], Mohamed Atrees[d], Abdelfatah Farag[a], Emad Elshehy[d,*], and Amr M. Abdelkader[e,*]

[a]*Department of Chemistry, Faculty of Science, Helwan University, Cairo, Egypt*

[b]*Department of Chemistry, Faculty of Science, Assiut University, Assiut, 71516, Egypt*

[c]*University of Jeddah, College of Science, Department of Chemistry, P.O. Box 80327, Jeddah 21589, Saudi Arabia*

[d] *Nuclear Materials Authority, P.O. Box 530, El-Maadi, Cairo, 11728, Egypt*

[e]*Department of Engineering, Bournemouth University, Talbot Campus, Fern Barrow, Poole, BH12 5BB, United Kingdom.*

Abstract: Here, we introduce a highly porous functional mesoscopically silica-polymer composite based on silica monolith-conjugated thiourea/formaldehyde copolymer. The developed nanostructure enables selective and fast removal of the radioactive pollutant strontium (Sr(II)) and cesium (Cs(I)) ions from contaminated seawater. The composite is synthesized by introducing thiourea/formaldehyde solution into tetramethoxy orthosilicate (TMOS)/triblock copolymer emulsion. The chemical and textural features of the synthesized silica/thiourea-formaldehyde polymer composite (SiO2-TUF) were characterized using Fourier transform infrared spectroscopy (FTIR), X-ray Photoelectron Spectroscopy (XPS), Scanning Electron Microscope (SEM), High-Resolution Transmission Electron Microscope (HRTEM), Energy Dispersive X-Ray Analysis (EDX), Dynamic Light Scattering (DLS), thermal analysis (TGA/TDA), and N_2 adsorption/desorption measurements. The synthesized microporous SiO2-TUF showed excellent cesium and strontium removal ability, reaching a maximum adsorption capacity of 78.2 and 40.3 mg g^{-1} for Sr(II) and Cs(I), respectively. When tested with seawater contaminated with radioactive cesium and strontium, SiO2-TUF was able to selectively target Sr(II) and Cs(I) ions. Among the different types of adsorption isotherms investigated, Sips isotherm showed the best fit with R^2>0.990. The kinetic studies showed that the pseudo-second-order model gave the best description of the uptake process.

Keywords: Porous Materials; Silica; Polymer; Adsorption; radioactive waste.

***Corresponding authors email address:** eelshehy@yahoo.com (Emad Elshehy) & aa494@cam.ac.uk (Amor Abdelkader).

1. Introduction

In the last few decades, there has been an increasing global concern about the environmental and public health consequences of decommissioning nuclear facilities that reach their end of service life. The post-operational cleanout (POCO) protocols are expected to generate a significant amount of waste effluent with various radioactive materials that needed to be treated and managed to eliminate their damaging effect.[1-6] The global concern magnified with the leaking of radionuclides to the seawater used for emergency cooling following the Fukushima accidents.[2, 4] The radioactive cesium-137 and strontium-90 ions are of particular concern due to its long half-life (28.78 and 30.17 years, respectively), mobility in the environment, and the spread of the serious hazards to the environment from their high-dosage emission.[7] In addition to the environmental hazards, cesium and strontium have detrimental impacts on human health and could contribute to morbidity and mortality worldwide. The high mobility of cesium in many biological systems allows it to deposit in the soft tissues all over the body and create an internal hazard like thyroid cancer, especially to the reproductive system.[8] Strontium is also linked to bone cancer leukaemia.[2] Therefore, it is important to develop an effective treatment system to remove cesium and strontium from contaminated seawater. However, cesium has a similar chemistry to that of sodium and potassium, and strontium resembles the chemistry of calcium, making the selective removal of cesium and strontium from contaminated seawater, not a trivial process.

Several techniques have been used for the removal of monovalent Cs(I) and divalent Sr(II) ions from contaminated nuclear waste solutions include; flocculation, co-precipitation, solvent extraction, evaporation, membrane filtration, biological remediation, electrocoagulation process, reverse osmosis, electrodialysis and adsorption.[5, 7-12] Among these, adsorption is one of the most influential and economical approaches, which has been adopted by many nuclear power plants around the world. Organic polymeric resins are still the most commonly used adsorbent in nuclear power plants. However, various inorganic

materials have shown promising results as adsorbents for Cs, and Sr ions include; natural and synthetic zeolites, graphene oxide, metal-organic framework, multiwall carbon nanotubes, activated carbon, clinoptilolite, silicotitanate, metal ferrocyanide, hydroxylapatite, mesoporous menotite and metal phosphates.[13-19] In recent years, adsorption processes that utilize inorganic-organic conjugates, including metal oxide/polymer composites, have attracted considerable interest due to their high removal efficiency, physical stability and low cost. Conjugated inorganic-organic nanocomposites take advantage of the synergy between organic polymers and inorganic nanoscale building blocks.[20] This synergy gives a unique set of properties such as rigidity and thermal stability of the inorganic component; and flexibility, dielectric and ductility of the polymer part. Concerning the adsorption applications, porous nanostructures based on transition metals oxides are at the forefront of the conjugated inorganic-organic candidates.[21-25] Mesoporous silica/organic nanocomposite possesses tunable pore sizes, uniform channel, and large surface area, making them promising candidates for solid-state adsorbent materials.[26-29] Mesoporous silica could be used to support the immobilization of ligand molecules without changing their functional activity or ability to capture the target metals ions. In this regards, mesoporous silica and high ordered mesoporous silica have been used for the removal of many toxic ions from water, including Cs and Sr. However, there is still a need for investigating the addition of specific functional groups that can enhance the materials ability to selectively attract Cs and Sr from a complex solution such as seawater.

Many attempts have been made to synthesis inorganic nanoparticle-filled polymer nanocomposites using a chemical approach. However, this approach requires overcome complicated polymerization processes, making them suitable for the industrial-scale production of nanocomposites. In this work, microporous silica incorporated thiourea/formaldehyde (TUF) polymer nanocomposite (SiO2-TUF) is prepared by entrapping the TUF polymer the triblock copolymer surfactant into the silica monoliths. The designed adsorbent was prepared via a simple process that allows the polymerization reactions to take place during the formation of the silica monoliths, resulting in hierarchical nanostructures nanochannels with a large specific surface area. The strong chemical bonding between the silica backbone and the groups in the

polymer chain satisfied a stable structure with numerous active sites available for the selective interaction with the Cs and Sr ions. Benefiting from the porous structures and the availability of the functional groups on the surface, SiO2-TUF was able to remove Cs and Sr ions with sorption capacity as high as 78.2 mg g^{-1} in less than 10 minutes. The adsorption mechanism and various kinetic models are studied to understand the target ions-SiO2-TUF interactions. Although this work is devoted to investigating the removal of Cs(I) or Sr(II), we believe the same facile synthesis method could be used to prepare several other silica-porous polymers composites that can be used to remove other toxic substances.

2- Materials and Methods

2.1. Materials

All materials were of analytical grade and used without further purification. Tetramethylorthosilicate (TMOS), the triblock copolymers of poly(ethylene oxide-b-propylene oxide-b-ethylene oxide) pluronic F108 [F108 ($EO_{141}PO_{44}EO_{141}$)], thiourea (TU), formaldehyde (F) were obtained from Sigma–Aldrich. Cesium nitrate ($CsNO_3$) and strontium chloride ($SrCl_2$) solutions (1000 mg L^{-1} in 0.05 M HNO_3) were purchased from Merck. The solution was further diluted to the required concentrations (1-100 mg L^{-1}) with deionized water (DIW). The pH of the solutions was adjusted using 0.01 M nitric acid or 0.01 M sodium hydroxide solutions.

2.2. Synthesis of SiO2-TUF composite

The silica/polymer nanocomposite (SiO2-TUF) was prepared using an instant, one-pot, direct templating method. This method is similar to our previously reported to prepare High Ordered Monoliths (HOM) silica monoliths, with in *situ* TUF polymerization.[29] Typically, silica monoliths were fabricated using microemulsion phases formed by the addition of the solution of thiourea and formaldehyde (pH 9) to F108 surfactant/TMOS) mixture domains. First, in a 100 mL beaker (beaker 1), 15.2 g of thiourea (0.2 M) and 20 mL absolute ethanol were mixed at 30 °C; then was added to 16.2 g of formaldehyde solution (0.2 M). The molar ratio of thiourea to formaldehyde used in this study was 1:1. The pH value of the solution mixture

was adjusted using NaOH until it reached up to 9. The mixture was heated at 75°C until all reactants were dissolved. Second, in beaker 2, Pluronic F108 and TMOS were mixed with 30 mL ethanol by agitation in a water bath (45 ºC) for 1–5 min, until a homogeneous sol-gel was produced. The mass ratio of F108: TMOS under typical conditions was 1.3: 1. Subsequently, the solution mixtures of beaker 1 and beaker 2 were charged into the round balloon flask. In microporous worm-like channels of silica/polymer syntheses, the flask containing the synthesis composition was instantly connected to the rotary evaporator (EYELA NVC-2100) at 45 ºC a starting pressure of 1023 hPa. An acid-catalyzed condensation reaction continued the syntheses by adding an aqueous HCl/H_2O solution (pH 1.3). In the acid condensation step, the exothermic hydrolysis and condensation of TMOS occurred rapidly, along with TUF condensates began to precipitate. After a 15-min evacuation, the resulting optical sol-gel-like silica/polymer material was formed with continuous polymerization of TUF/TMOS. This led to the formation of opaque SiO2-TUF monoliths (solid product) and acquired the shape and size of the round-balloon flask. The resultant surfactant-silica/polymer solid was gently dried at room temperature for 6 h and then allowed to stand in a sealed container at 25°C for 1 day to complete the drying process. Finally, the F108 of the as-made SiO2-TUF sample was removed by the solvent extraction method. After 24 h of solvent extraction with ethanol, the SiO2-TUF material was dried at 75 °C, ground and stored for use as adsorbent materials for Cs(I) and Sr(II) removal.

2.3. Characterization instruments

The FTIR spectra for the synthesized materials were measured using Pye-Unicam Sp-883 PerkinElmer spectrophotometer, (Waltham, MA, USA). The morphology of microporous SiO2-TUF composite particle was examined by scanning electron microscopy (SEM) using a Jeol JSM-5400 LV instrument. TEM micrographs of the free HOM-silica and microporous SiO2-TUF composite were achieved using a JEOL JEM-1400 transmission electron microscope (JEOL, Ltd, Tokyo, Japan). The specific surface and porosity were measured using nitrogen adsorption (BELSORP MIN-II analyzer) at 77 K (MicrotracBEL Corp., Osaka, Japan). Particle size distribution and zeta potential of SiO2-TUF composite were determined

by dynamic light scattering using a Nano Series Zeta Sizer (Malvern, Worcestershire, UK). The TGA/DTG analyses were acquired on a Shimadzu DT = TG-50 thermogravimeter, under N_2 atmosphere (Shimadzu, Kyoto, Japan). Finally, Cs(I) and Sr(II) ions were quantified via an Inductively Coupled Plasma-Optical Emission Spectrometer (ICP-OES, model 720-ICP-OES, Agilent Technologies).

2.4. Batch studies for Cs(I) and Sr(II) ions adsorption assays

Sorption tests were carried out using batch experiments. A fixed amount of SiO2-TUF, W = 20 mg) was mixed with a volume of solution (V = 20 mL) containing Cs(I) or Sr(II), at concentration C_0: 50 mg/L (sorbent dosage, 1 g/L). The initial pH of the solution was varied between 1 and 11 with HNO_3 or NaOH solutions. The flask was maintained under agitation (300 rpm) for 120 min at different temperature (25°C, 35°C, and 45°C). The solution was separated from SiO2-TUF microporous sorbent by filtration on an Ahlstrom glass microfiber filter paper (1.2 mm pore size; 4.7 cm diameter). ICP-OES measured the residual concentration of the target metal ions (C_e, mg/L) in the filtrate, and the sorption capacity (q_e, mg/g) was deduced from the mass balance equation:

$$q_e = [(C_i - C_e) \times \mathrm{V}]/W \quad (1)$$

Other experiments such as uptake kinetics, sorption isotherms, thermodynamic studies and the study of the effect of co-existing ions were conducted under the same procedures. Intermediary samples were collected for uptake kinetics, while initial concentrations were varied up to 125 mg/L (at pH 8 and 6 for Cs(I) and Sr(II), respectively) for sorption isotherms. For the study of the effect of co-existing ions, the target metal ion solution (1 mg/ L) was added to different interfering ions (at the concentration of 5 mg/L), other experimental conditions being identical.

Regeneration of SiO2-TUF was conducting through submerging 0.1g of the SiO2-TUF composite in 50 mL of 100 mg/L Cs(I) or Sr(II) solution under optimal experimental conditions. The solution was filtrated, and the loaded SiO2-TUF composites with Cs(II) and Sr(II) were washed with demineralized water, and then undergo to elution with 0.02 M HNO_3 (20 mL). The recovery efficiency (R_E %) was obtained from Eq. (2);

$$R_E\,(\%) = [(q_1 - q_2)/q_1] \times 100 \quad (2)$$

where (R_E) is the recovery efficiency (%), while q_1 and q_2 are the sorption capacities at the 1st and 2nd run, respectively. Sorption and desorption efficiencies were compared for eight successive cycles. The application efficiency of the SiO2-TUF for Cs (I) and Sr (II) removal from seawater was tested on a seawater sample collected from the Mediterranean Sea close to Alexandria Governorate (Egypt). The solutions were spiked with 1 mg/L Cs (I), Sr (II) and Rb(I) ions.

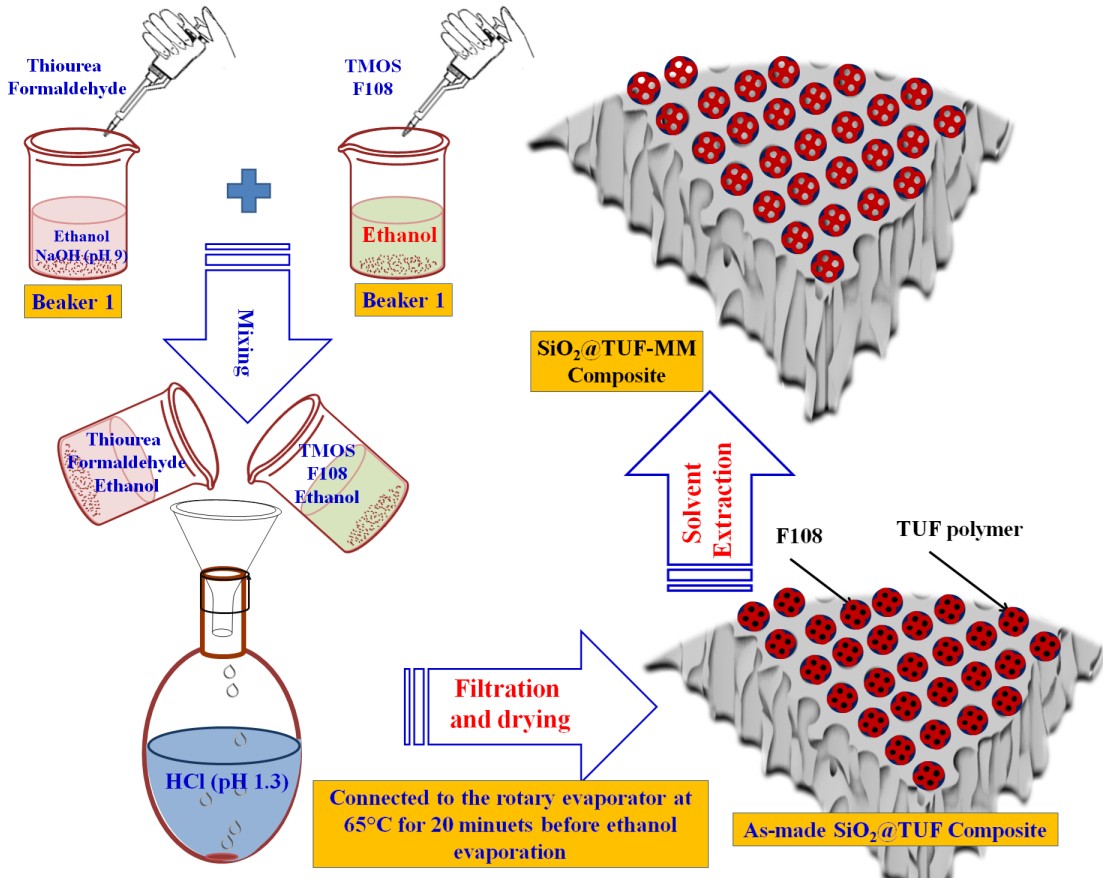

Scheme 1: Schematic representation of the preparation procedure

3. Results and discussion

3.1. Characterization of SiO2-TUF composite

This SiO2-TUF composite was synthesized by emulsion-compounding each of the silica, surfactant, and monomers in a mixture of ethanol/acetic acid solution having different hydrophilic characteristics with appropriate ratios. The fabrication process of the porous hybrid SiO2-TUF is illustrated schematically in scheme 1. The intercalation of TUF polymer into the organically modified layered silicate and the subsequent surfactant removal from the silicate/polymer frameworks was performed using a solvent extraction technique. Pluronic F108 is a tri-block copolymer with a terminal primary dihydroxy-functional oligomer, which lead to a directional arrangement on the surface of the solution. The oxygen atoms of the tri-block copolymer surfactant can interact with the terminal hydroxyl methyl groups of TUF oligomers, forming hydrogen bonds inside the polymers molecule.[30] Some hydrogen bonds can also exist between the nitrogen atoms of TUF oligomers and hydrogen atoms of tri-block copolymer surfactant. The synthesis mechanism of SiO2-TUF ensures the polymerization process, and the strong molecular forces between TUF oligomers and the surfactant is taking place inside the silica pores. As a result, porous silica monoliths are the matrix that hosts the F108/TUF in its pores. This porous silica works as a backbone to give mechanical integrity and stability to the SiO2-TUF hybrid, allowing for high Cs(I) and Sr(II) ions adsorption capacities after surfactant removal. The scanning electron microscope (SEM) micrograph shows the stable micrometre-scale morphology (≥1 μm) consisting of agglomerates or different non-uniform particles of synthesized SiO2-TUF monoliths (Fig. 1).

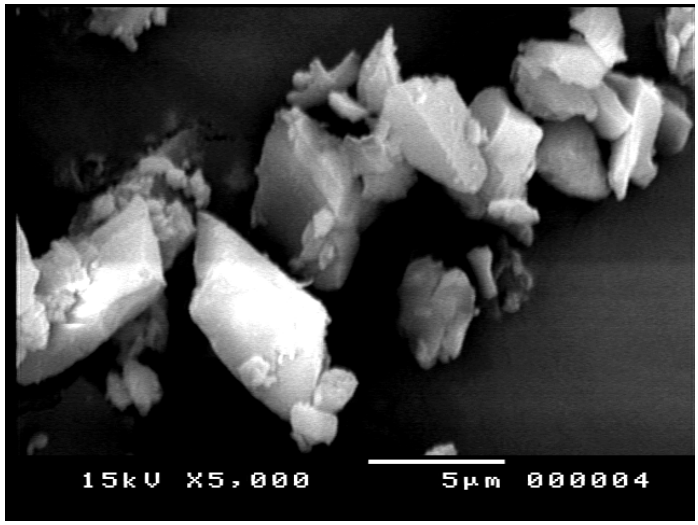

Figure 1: FESEM images of the synthesized SiO_2-TUF composite and the optical photograph after crushing.

TEM micrograph (Fig. 2(a)) of the SiO_2-TUF monoliths showed that the silica/polymer particle formed large aggregates. TEM micrograph of the as-synthesized SiO_2-TUF shows the flacks on the composite surface with homogeneous distributions along the entire surfaces (Fig. 2(b)). It can be seen that the surface of the silica/polymer composite after surfactant removal did not show the structural organization of pores, meaning that the addition of thiourea/formaldehyde monomers changed the micelles structure and pore networks (Fig 2(c&d). Where the external surface of the silica monoliths (without polymer) show, visible high ordered cubic mesopores distributed uniformly across the entire surfaces with a regular diameter in the range of 25-30 nm (Fig. 2(e&f)). The STEM-EDS analysis reveals a uniform distribution of the hybrid elements, including S and N (Fig. 3). The elemental composition can be determined for SiO_2-TUF composite to be 16.57% (C), 3.34% (H), 12.77% (N), and 12.33% (S). The Nitrogen and sulfur contents were found to be 9.12 and 3.85 mmol per gram of SiO_2-TUF nanocomposite, respectively.

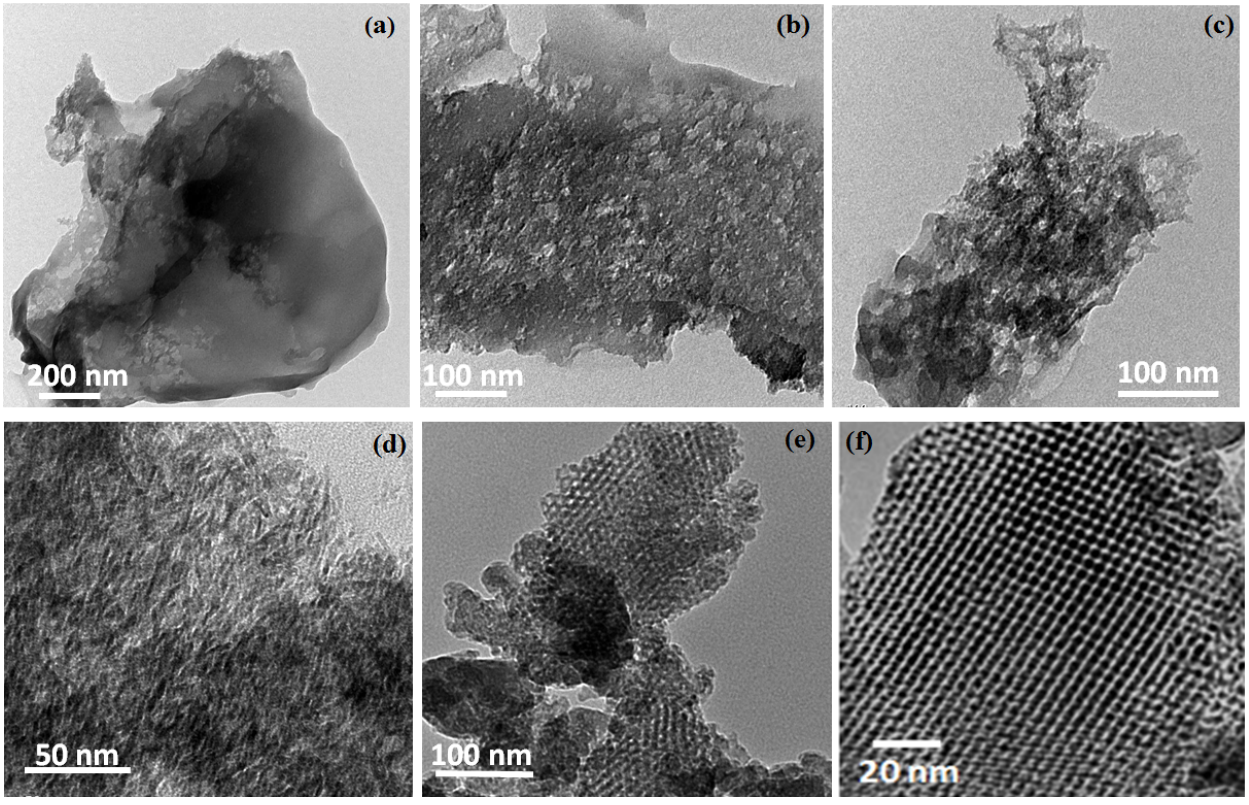

Figure 2 TEM images of as-synthesized SiO2-TUF composite (a&b), the synthesized SiO2-TUF after surfactant removal (c&d), and the silica monolith without TUF polymer incorporation (e&f).

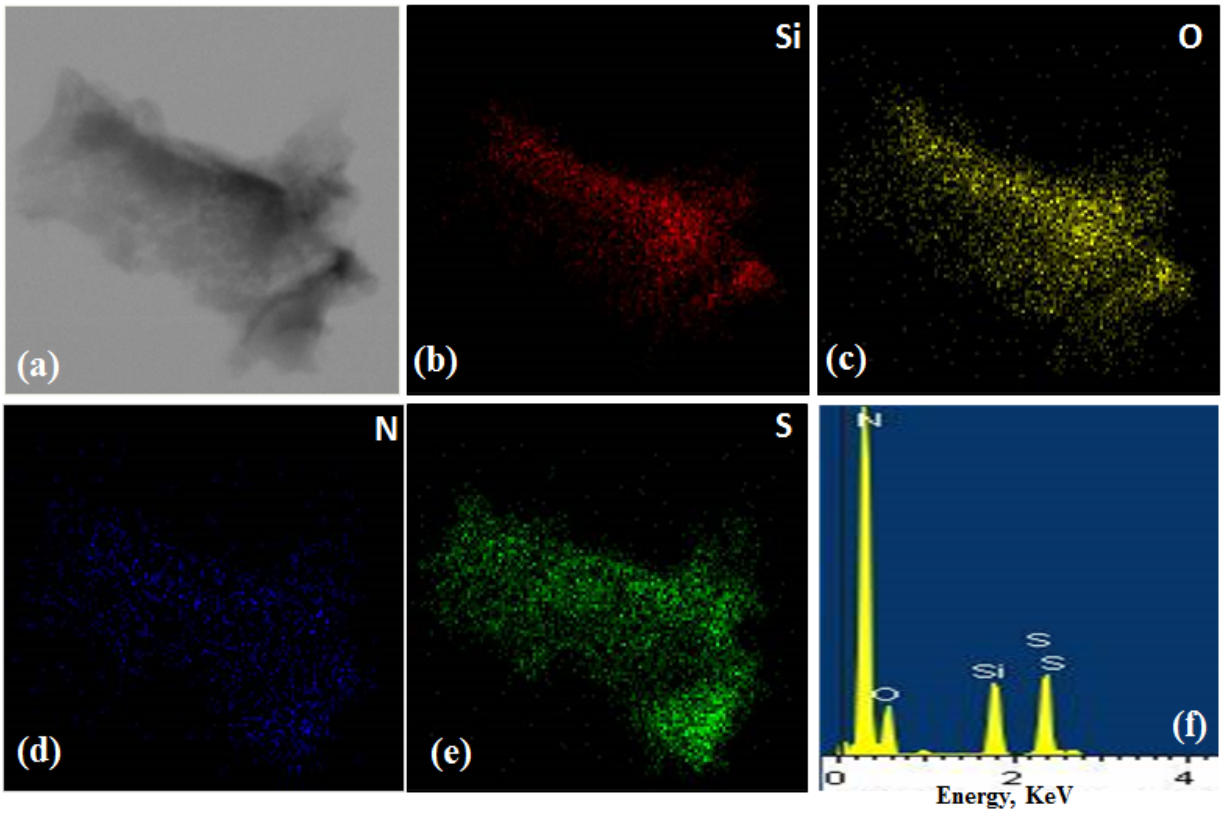

Figure 3: STEM image (a), EDS elemental mapping (b–e), and (f) EDS spectrum of the microporous SiO2-TUF.

More information about the porosity characteristics of the SiO2-TUF nanocomposite can be gathered from the N_2 adsorption/desorption technique (Fig. 4a). The calculated BET surface area of the SiO2-TUF is 815.71 m^2 $g^{-1,}$ and the total pore volume is close to 0.7627 cm^3 g^{-1}, with micropores centred at about 1.87 nm. For comparison, a controlled high ordered mesoporous polymer-free silica monolith (HOM-silica) exhibits a specific surface area of only 400 m^2/g and mesopores in the range up to 30 nm. The N_2 adsorption/desorption isotherm shows a typical IV type with a hysteresis loop at low P/P_o with a typical hysteresis loop H1 implies uniform cylindrical pore geometry. In addition, this isotherm type is often obtained with materials consisting of agglomerates or different non-uniform particles, as evidenced from SEM images (Fig. 1).[31] The SiO2-TUF exhibits capillary condensation at a relative pressure of about 0.25, attributed to some pore blocking. The isotherm's steepness and the occurrence of capillary evaporation are

associated with the formation of uniform pore diameter. Embedding the polymer into silica mesopores did not block the porous backbone completely but rather tailored the hybrid into 3-dimensional (3D) micropores architectures after surfactant removal. From our results, the pore size distribution shows mean pore diameters of 1.87 nm in which small channels were formed between large uniform pores (30 nm). This was confirmed from ordered pores appear in HRTEM image (Fig. 2(F)) of pristine silica, that each particle observed had ordered mesoporous arrays with clearly feature open, connected pores and continuous (channels) with regular structures. Meanwhile, the number of pores on the particle also affected the increasing specific surface area. The more pores, the larger the specific surface area. The pore volume of SiO2-TUF was 0.7627 $cm^3 g^{-1,}$ and the pore volume of pristine silica was 0.4855 $cm^3 g^{-1}$, which was half lower than pristine silica. The larger pore volume resulted from the SiO2-TUF having many more pores.[32] So, we can conclude that the incorporation of TUF polymer have an influence on the surface area where F108/ can serve as a dual template in order to form the many nanochannels inside the silica matrix after surfactant removal. Therefore, it was not difficult to understand that the specific surface area for the SiO2-TUF was more significant than the HOM-silica particles.

TGA/DTG techniques determined the carbon content and the thermal stability of the SiO2-TUF. TGA curve (Fig. 4b) displays a total weight loss of 65.84 % in the temperature range 35–1000^{o}C (Fig. 3b), in which various stages can be identified in the thermogram. First, about 4.245% weight loss is observed between 35°C and 120°C, associated with the release of trapped solvent and absorbed water. The decomposition and pyrolysis of thiourea/formaldehyde polymer are taking place in two steps; one associate with a fast loss of 34.69% of the sample mass at ~ 300°C, and a gradual loss of about 21.81% between 300°C to 470 °C. The last thermal process is observed at a temperature above 500°C with a gradual weight loss of about 5.1%. These different thermal transformations are correlated to three maximum peaks on the DTG curve: at 57.08°C, 224.81°C and 637.16°C correspondings to dehydration, degradation, and crystalline phase formation of silica monoliths, respectively. From the dynamic light scattering (DLS) analysis (Fig. 4c), the SiO2-TUF exhibits a uniform size in the range of 130-160 nm in diameter, suggesting the formation of sub-micron particles of SiO2-TUF. The surface zeta potential of Silica@TUF was determined to be −15 mV (Fig. 4d).

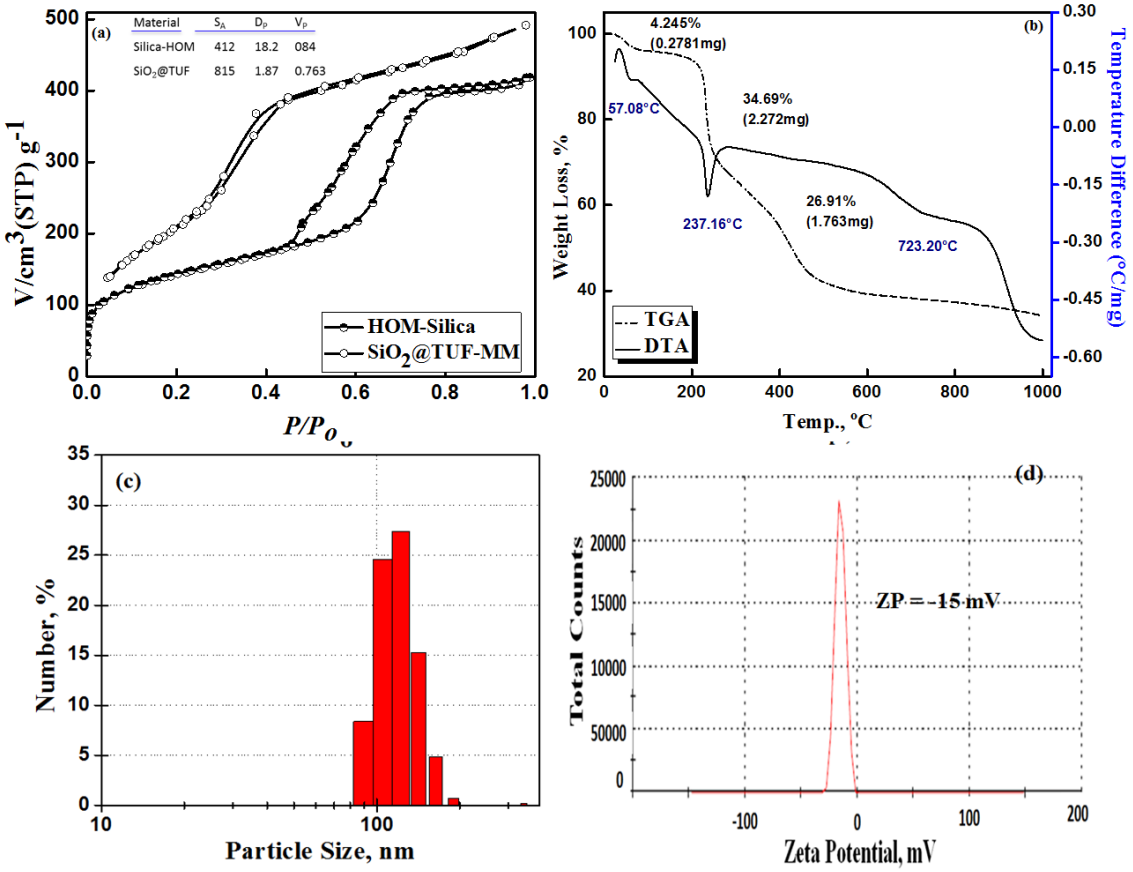

Figure 4: (a) N_2 sorption/desorption isotherms of the synthesized SiO2-TUF after surfactant removal and the silica monolith without polymer incorporation, (b) TGA and DTA, (c) particle size distribution, and (d) zeta potential of the microporous SiO2-TUF particles.

The chemical composition and the surface functional groups of the silica monoliths and the SiO2-TUF were determined by FT-IR and XPS analysis. FT-IR spectrum of the silica monoliths (Figure S1) displays a number of characteristic bands; the peak at ~1090 is for the siloxane backbone (Si–O– Si), the 961 band is for the free silanol group (Si–OH), and the peak at 804 cm^{-1} is characteristic for the tetrahedron ring in (SiO_4).[33] In addition to the silica peaks, the FT-IR spectrum of the SiO2-TUF shows some new characteristic bands. The peak at 1619 cm^{-1} is associated with the $–NH_2$ vibration, and the peak at 1150 cm^{-1} is for the (C=S) vibrations. Two strong bands appeared at 3020 and 2980 cm^{-1} due to the asymmetrical and

247 symmetrical stretching vibrations of the $–CH_2$ groups and another band at 1440 cm^{-1}, assigned to the δ(C–
248 H) bending of $N–CH_2–N$.[34] The presence of coordinated water molecules in the composite was further
249 confirmed by the appearance of bands in the region 1530 cm^{-1} for δ(HOH) deformation and the band at 650
250 cm^{-1} for the rocking modes of coordinated water.[35] The Si-S and Si-N bands at 655 cm^{-1} and 525 cm^{-1},
251 respectively, confirm the reaction between the polymer and the silica.[36] The successful incorporation of the
252 TUF polymer into the silica monoliths is further confirmed with the high-resolution XPS spectra. Fig. 5
253 shows that the chemical incorporation of SiO2-TUF composite introduces S/N-based reactive groups (due
254 to thiourea/formaldehyde inclusion). The figure identifies the different forms associated with C, S, O, N,
255 and Si elements in their different chemical environments, indicating that the SiO2-TUF was synthesized
256 successfully. The C 1s can be fitted with four peaks at 284.48, 285.89, 286.73, 286.6, and 287.67 eV
257 corresponding to the C-O, C-N, C-S, N-C-N species, respectively. The S2p spectrum exhibited three
258 binding energies of 161.2, 161.9, and 162.34 eV are associated with C–S, S=O and S–S bonds (i.e. during
259 the synthesis of SiO2-TUF, thiourea is involved in the reaction, and the product containing thioether bond
260 and disulfide bond).[35,36] The co-existence of protonated and protonated amine groups (at similar atomic
261 fractions) is also demonstrated by the presence of two deconvoluted peaks at 399.15 and 401.08 eV,
262 respectively.

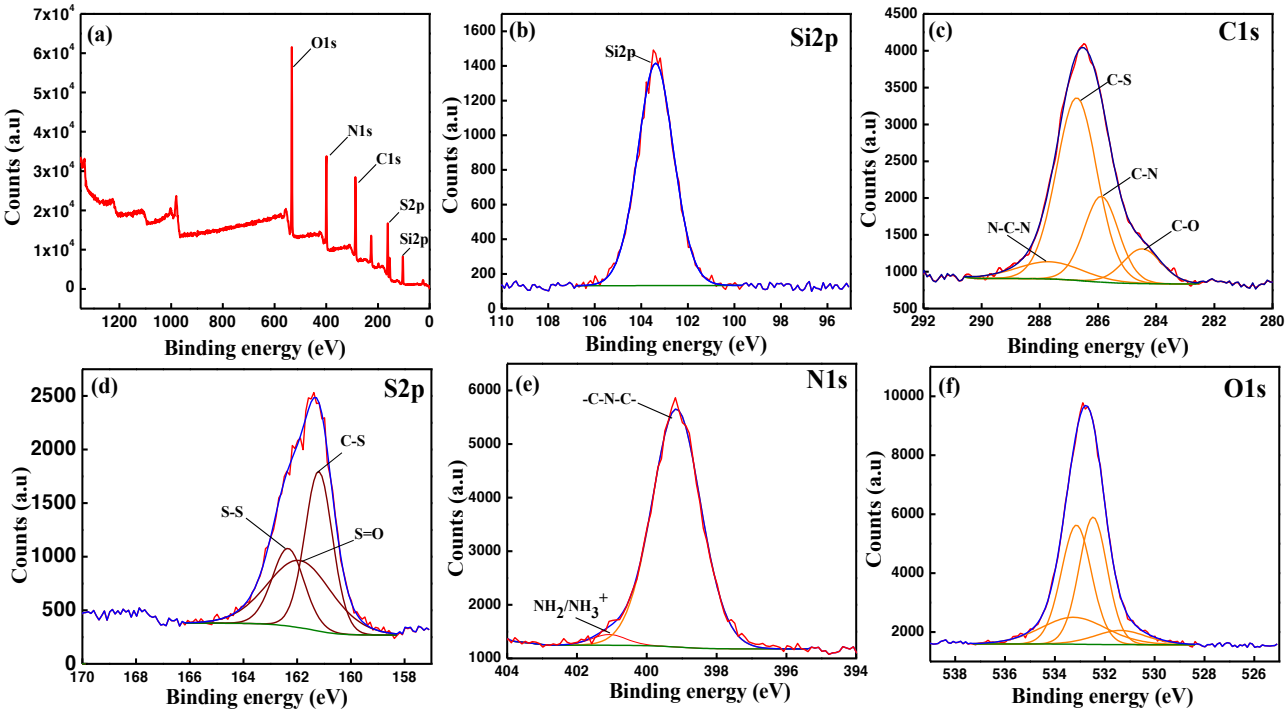

Figure 5: XPS spectra of the synthesized microporous Silica@TUF composite.

3.2. Cs(I) and Sr(II) adsorption

3.2.1. effect of pH

For any adsorption system, the solution's initial pH could result in fundamental changes in the adsorbent by alternating the surface charges or changing the types of ions in the solution. The presence of thiol and amino group on the SiO2-TUF suggests that the first reaction in acidic media would be the surface groups' protonating according to reactions 3 and 4. Zeta potential is an important parameter for understanding the mechanism of adsorption. It is the electrical potential close to a particle surface where adsorption of ions from the solution phase occurs, and it is positively related to the surface charge. Furthermore, zeta potential depends not only on the particle's surface properties but also on the nature of the solution (e.g. ionic strength, pH, etc.). The surface zeta potential of SiO2-TUF was determined to be −15 mV (Fig. 3d). The negative value is due to the deprotonated groups (-OH, -SH, and -NH_2) of the silica-TUF polymer composite that can explain the pH variations of uptake of Cs(I) and Sr(II) ions from solution by SiO2-TUF. We studied the influence of the initial pH value on Cs (I) adsorption (I) or Sr(II) at room temperature by fixing the ions

277 concentration at 50 mg L^{-1}. As can be seen in Figure 6a, the adsorption capacity of Cs(I) on SiO2-TUF
278 reaching a maximum value of 16.2 mg g^{-1} at pH values between 7- 8.5. Sr(II) 's adsorption capacity is higher
279 than that of Cs(I) at all the pH values and plateauing at a maximum value of 34.7 mg g^{-1} starting at pH
280 values as low as 4. The observed lower uptake values for Cs(I) and Sr(II) ions at lower pH values (pH≤4)
281 is due to the formation of hydronium ions on the SiO2-TUF surface. These ions render the sorbent's charge
282 to be mainly positive (equation 5),5 hindering the interaction with the solution cations and hence decreasing
283 the adsorption capacity. The decrease of the metal uptake at higher pH values in the case of Sr(II) is due to
284 the formation of insoluble complexes that causes some precipitation of strontium. The maximum adsorption
285 capacity of strontium on SiO2-TUF occurred at a pH of 6 without any strontium precipitation from the
286 solution.[18, 37] On the other hand, the decrease of the uptake of Cs(I) ions at high pH is due to the formation
287 of soluble CsOH on the sorbent surface.[4] The differences between sorption capacities of the Cs(I) or Sr(II)
288 may be explained by the higher ionic strength of Sr(II) and also the smaller size of the ions, allowing Sr(II)
289 to accesses smaller pores. All subsequent adsorption experiments of Cs(I) and Sr(II) ions on the
290 microporous SiO2-TUF were performed at pH 8 and 6, respectively, to evaluate other adsorption
291 parameters.

292 $$RNH_2 + HCl = RNH_3^+Cl^- \quad (3)$$

293 $$RSH + HCl = RSH_2^+Cl^- \quad (4)$$

294 $$H_2O + H^+ = H_3O^+ \quad (5)$$

295

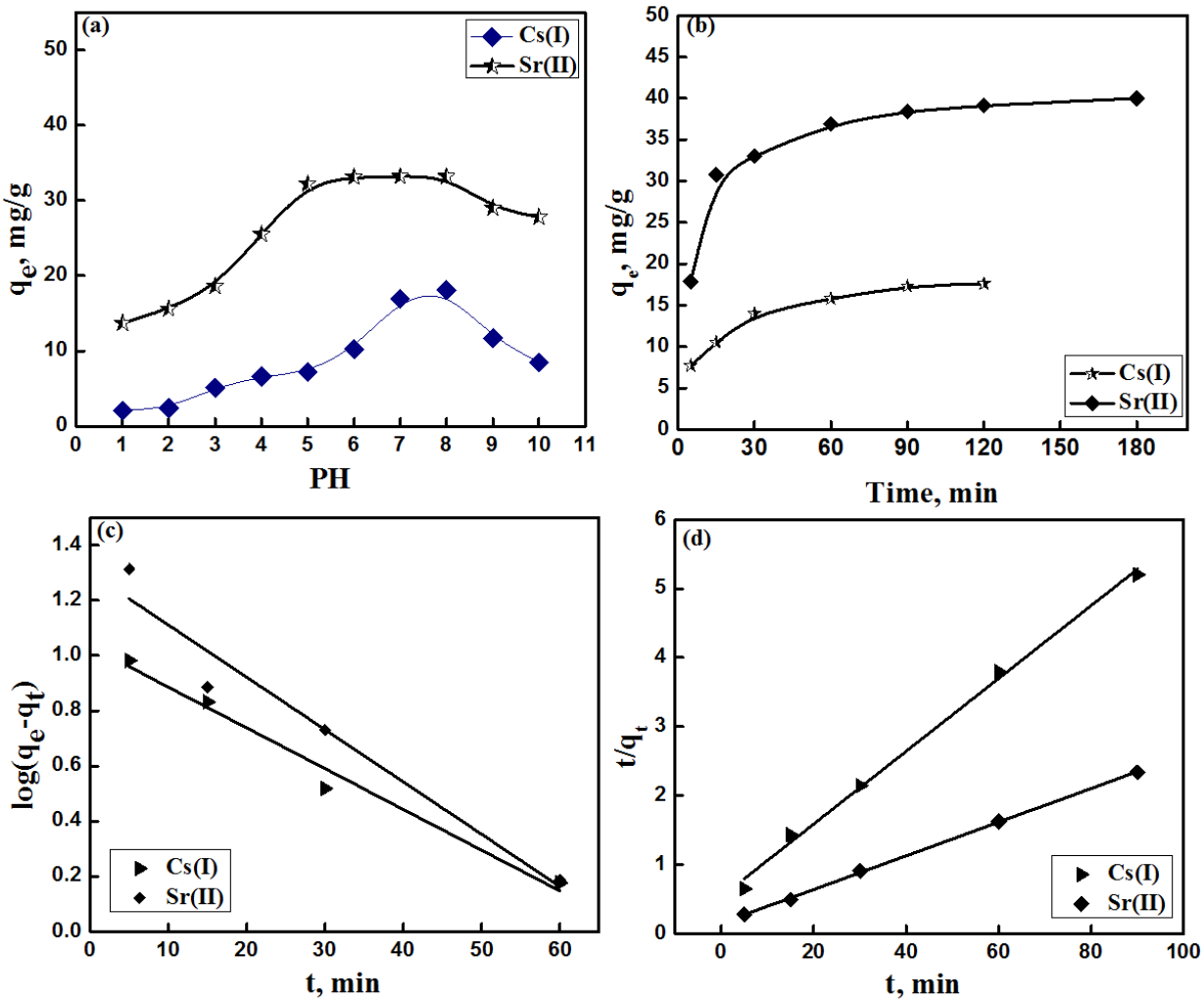

Figure 6: Effect of pH on the adsorption of U(VI) and Cs(I) ions on SiO2-TUF; initial metal ion concentration 100 mg L^{-1}, SiO2-TUF weight 20 mg, solution volume 20 mL, eq. time 90 min at temp. 25 °C.

3.2.2. Adsorption kinetics

The first clue of the adsorption reactions kinetic is given by Figure 6b. The time of equilibrium measured at the specified pH values and 50 mg L^{-1} is about ~40 min for Sr(II) and ~25 min for Cs(I). Within ten minutes, the uptake efficiency reaches 55.6% and 62.8% from the total uptake capacities for Sr(II) and Cs(I), respectively, indicating a fast adsorption process. The longer time required to reach equilibrium for Sr(II) is understood from the relatively smaller cations' ability to diffusion through the pores of SiO2-TUF.

Also, the smaller cations of Sr, Sr2+ and SrOH+, seem to diffuse through the electric double layer (EDL) formed on the surface. The ability to penetrate through the EDL, although fulfil higher capacity, would mean the uptake process is not purely controlled by a fast surface adsorption process but rather with a slow diffusion step.

The kinetics of the adsorption process is further studied using several models. We first used the conventional pseudo-first-order (PFORE) and pseudo-second-order (PSORE) rate equations to fit the kinetic profile (equations 6 and 7). [39]

$$log(qe - qt) = log(t) - \frac{k_1}{2.303}(t) \qquad (6)$$

$$t/q_t = t/q_2 + 1/k_2 q_2^2 \qquad (7)$$

Where q_e is the adsorption capacity, k_1 and k_2 are the apparent rate coefficients for PFORE and PSORE, respectively. Plotting $log(q_e-q_t)$ versus t (Fig. 6c) and plotting t/q_t versus t (Fig. 6d) gave straight lines. The theoretical capacities and rate constants can be calculated from the slope and the intercept of the lines. The correlation coefficient obtained from the linear correlation coefficient (R2) confirmed the models' validities. In general, the closer the value of R^2 to 1, the better the model on describing the kinetic data. Table 1 reports the parameters of the models fitting to experimental curves. The determined R^2 value of the PSORE is slightly higher than that of PFORE for both Sr(II) and Cs(I), suggesting that both metal ions' sorption rate into the SiO2-TUF is better modelled with the second-order model. Since PFORE is supposed to fit profiles controlled by physical sorption while the PSORE is usually associated with chemical sorption, the results in table 1 suggest a more chemically controlled process. Therefore, the adsorption process can be considered to proceed through the following steps; bulk diffusion, film diffusion, pore diffusion and chemical reaction. To gain more insight into the sorption kinetic, other models are considered. McKay model assumes that the adsorption process is controlled by the film- and particle diffusion.[39] During the transport of the solute species from the bulk liquid phase towards the solid adsorbent surface, the boundary layer may play a

significant role in the adsorption process. This may be verified by applying the adsorption time data to the liquid film diffusion model:[38]

$$log(1 - F) = - K_F/2.303\ t \quad (8)$$

Where K_F is the film diffusion rate constant (min^{-1}), and F is the ratio q_t/q_e. Plotting *log(1-F)* versus *t* gives a straight line that passes through the origin for a process controlled only by ions diffusion through the double layer film (Fig 7a). The rate constant for liquid film diffusion (K_F) was determined to be 0.0345 and 0.044 for Cs(I) and S(II), respectively. However, the resulting lines in both cases have a non-zero intercept, indicating that the film diffusion is not fully responsible for determining the adsorption rate on SiO2-TUF. Further, we fitted the time dependence data of Cs(I) and Sr(II) adsorption using Weber-Morris model, which assumes the processes is controlled by intra-particle diffusion.[38, 39] This model state that the intra-particle diffusivity is constant and the direction of the diffusion process is radial;

$$q_e = x + K_i\ t^{1/2} \quad (9)$$

where K_i (mg g^{-1} $min^{-0.5}$) and *x* are the intera-particle diffusion rate constant and constant proportional to the boundary layer thickness, respectively. The values of K_i and *x* were determined from the slope and intercept of the plot of q_t versus $t^{1/2}$ (Fig. 7b). The high values of *x* (3.23 and 9.12 for Cs(I) and Sr(II), respectively) indicate that the boundary layer thickness plays a role in the adsorption process. It is evident from the plots that there are two separate stages; the first linear portion (stage I) and the second curved path followed by a plateau (Stage II). In Stage I, the removal efficiency reaches 55.6% and 62.8% from the total uptake capacities for Sr(II) and Cs(I), respectively, within 10 min. This is attributed to the immediate utilization of the most readily available active sites on the SiO2-TUF surfaces. In stage II, very slow diffusion of the target metal ions from the surface site into the SiO2-TUF micropores is observed. Thus, the initial portion of target metal ion adsorption on SiO2-TUF may be governed by the initial intraparticle transport of Cs(I) and Sr(II) ions controlled by the surface diffusion process. The later part is controlled by pore diffusion.[40] Though intraparticle diffusion renders straight lines for adsorption of Cs(I) and Sr(II) on

353 the synthesized SiO2-TUF, the intercept of the lines fails to pass through the origin. One possible
354 explanation is the difference in the rate of mass transfer between the initial and final stages of the adsorption.
355 It indicates some degree of boundary layer control which implies that intraparticle diffusion is not only the
356 rate-controlling step. The data were further used to learn about the slow step occurring in the present
357 adsorption system using the pore diffusion model using Bangham's equation which describes pore diffusion
358 during the adsorption process. This model assumes that the diffusion of metal ions into the micropores of
359 SiO2-TUF is the rate-controlling step; [40, 41]

360 $$log\left({C_i}/{C_i - Aq_t}\right) = log\, log\left({AK_B}/{2.303\, V}\right) + B\, log\ \mathrm{t} \qquad (10)$$

361 Where β and K_b (mL/g/L) are Bangham constants and A is the weight of SiO2-TUF per litre of cesium
362 solution (g L^{-1}). The straight line with a higher correlation value of the Bangham model (Fig. 6c) confirms
363 the adsorption process is controlled by diffusion within the pores. A similar trend was observed in the
364 literature for the adsorption of other ions onto porous materials.[41]

365 Another model that we have tested is the Elovich model, which is usually applicable for situations where
366 the rate determent step is the interaction between metal ions and the active adsorbent sites. The adsorption
367 data were treated according to Elovich equation;[41]

368 $$q_t = \frac{1}{\beta} ln(\alpha\beta) + \frac{1}{\beta} ln(t) \qquad (11)$$

369 where α is the initial adsorption rate (mg/g. min), and β is the adsorption constant (g mg^{-1}). The large
370 difference between the calculated values α and the experimental q_e indicates that the adsorption of Cs(I)
371 and Sr(II) on SiO2-TUF does not follow the Elovich model (Fig. 6d). Based on the above discussion, it
372 can be concluded that the adsorption of Cs(I) and Sr(II) on SiO2-TUF is best described by both McKay and
373 Bangham models. Therefore, the kinetics of the adsorption process is controlled by the diffusion of the ions
374 in the electric double layer surrounding the adsorption and also by the diffusion in the micropores.

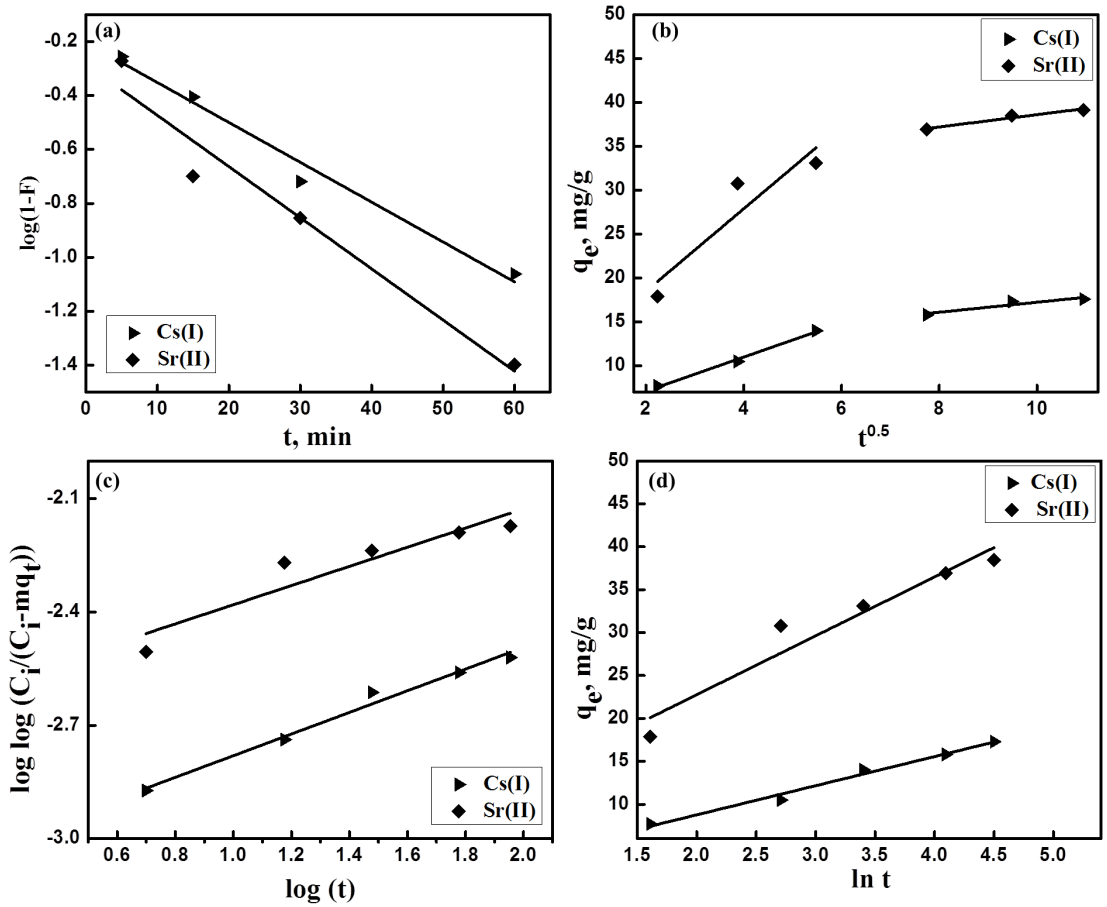

Fig. 6 (a) Effect of contact time on the adsorption of Sr(II) and Cs(I) ions at pH 8.0 on SiO2-TUF from a single ion solution; initial conc. 50 mg/L, adsorbent weight 20 mg, solution volume 20 mL at 25°C. (b) the pseudo-second-order plot.

Table 1. Kinetic Data for the Adsorption of Cs(I) and Sr(II) ions on SiO2-TUF microporous sorbent.

Kinetic Models	Kinetic Parameters	Cs(I)	Sr(II)

PFORE model	q_1 mg/g	10.7	17.3
	K_1 min-1	3.4×10^{-2}	4.4×10^{-2}
	R^2	0.973	0.933
PSORE model	q_2 mg/g	40.9	18.86
	K_2 mg^{-1} min^{-1}	0.0053	0.0039
	R^2	0.995	0.999
Weber-Morris diffusion model	K_{ip} [mg/(g $min^{0.5}$)]	1.94	4.69
	X	3.23	9.12
	R^2	0.990	0.730
Elovich kinetic model	β (g/mg)	0.294	0.146
	α [mg/(g min)]	6.08	25.62
	R^2	0.983	0.913
Liquid film diffusion model	K_F min^{-1}	0.034	0.045
	R^2	0.973	0.933
Bangham kinetic model	K_b (mL/g/L)	5.66	13.49
	α	0.286	0.254
	R^2	0.979	0.888

3.2.3. Adsorption isotherms

In order to evaluate the maximum sorption capacity of the microporous SiO2-TUF, adsorption isotherms were constructed using the data gathered at room temperature and pH values of 6 and 8 for Cs(I) and Sr(II), respectively. As can be seen from Figure 8, the uptake of the ions on silica@TUF sharply increases before reaching a saturation plateau at a maximum adsorption capacity of 40.3 and 75.5 mg g^{-1} for Cs(I) and Sr(II), respectively. We have used different isotherm models to explain the sorption process, such as Langmuir, Freundlich, and Sips models.[38-40] The Langmuir model assumes the adsorption occurs as a homogeneous monolayer on the sorbent surface and that the sorption capacity at saturation of this monolayer should correspond to maximum sorption capacity.[41] Since the correlation coefficient value (R^2) is low, it is safe to assume that the adsorption of Cs(I) and Sr(II) on SiO2-TUF does not obey Langmuir isotherm. The nonlinear Freundlich model[42] is described by a power-like equation, which is not consistent with the saturation plateau observed in Fig. 7. Sips isotherm is a combined form of Langmuir and Freundlich expressions deduced for predicting the heterogeneous adsorption systems and circumventing the limitation of the rising metal ions concentration associated with the Freundlich isotherm model. At low metal ions concentrations, it reduces to Freundlich isotherm, while at high concentrations, it predicts a monolayer adsorption capacity characteristic of the Langmuir isotherm.[43-45] As a general rule, the equation parameters

399 are governed mainly by operating conditions such as the alteration of pH, temperature, and concentration.
400 Therefore, we focused more on Freundlich the Sips model (Eq. 12 &13).

401 $$q_e = K_F\, C_e^{1/n} \quad (12)$$

402 $$q_e = \frac{Q_S K_S C_e^{n_S}}{1+K_S C_e^{n_S}} \quad (13)$$

403 where q_S (mg/g), K_F ($L^{1/n}$ $mg^{(1-1/n)/}g$) and K_S (L/mg), are the Sips sorption capacity and the affinity
404 coefficients for the Freundlich, and the Sips equations, respectively. The parameters n_F and n_S are the energy
405 coefficients for the Freundlich and the Sips equations, respectively. Values for 1/n close to zero indicate
406 heterogeneous adsorbents, while values closer to or 1.0 indicate a material with relatively homogenous
407 binding sites. It can be seen from Table 2 that the fitting parameters and the values of correlation coefficient
408 (R^2) suggest that the adsorption of Cs(I) and Sr(II) on SiO2-TUF is better described by the Freundlich and
409 Sips models (Table 2). It was clear that both two-parameter Freundlich and three-parameter Sips isotherms were
410 the best-fitting models for the experiment results where R^2 are nearly close. Therefore, the Chi-square statistic, X^2,
411 was also obtained and was shown in Table 2. The small number of χ^2 indicates that data from the model is close to
412 the experimental data. Whereas a large number of χ^2 suggests that data from the model is different from experimental
413 data. Therefore, there is a need to analyze the data using the chi-square test to confirm the best-fit isotherm for the
414 sorption system.[46] According to the χ^2 values (Table 2), the best-fit isotherm model was the Sips isotherm model,
415 where it exhibited lower χ^2 values than the Freundlich isotherm.

416

417

418

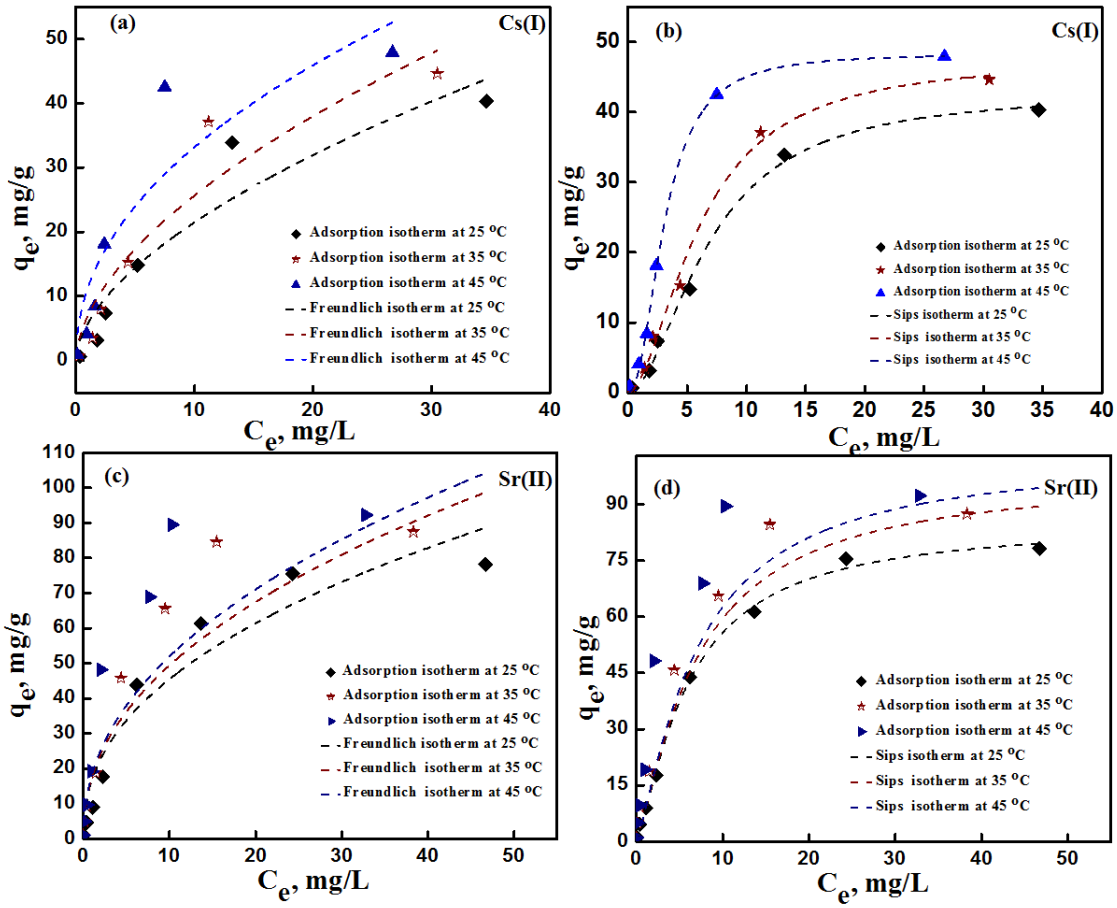

Fig. 8 (a&b) Freundlich isotherms and Sips isotherms of Cs(I) ions at different temperature (pH 8 , eq. time 45) and (c&d) Freundlich isotherms and Sips isotherms of Sr(II) ions at different temperature (pH 6, eq. time 60) (pH 6.0, eq. time 60) on SiO2-TUF from a single ion solution; SiO2-TUF weight 20 mg, solution volume 20 mL.

Table 2. Parameters of Freundlich and Sips models for Cs(I) and Sr(II) adsorption isotherms at different temperatures.

Metal ion	Temp.	q_e, mg L^{-1}	Freundlich				Sips				
			K_F	n_F	R^2	X^2	Q_S	K_S	n_S	R^2	X^2
Cs(I)	25°C	40.3	1.74	5.75	0.889	123.2	42.8	0.029	1.83	0.993	0.155
	35°C	44.6	1.77	6.97	0.891	146.2	47.7	0.039	1.80	0.991	0.215
	45°C	48.4	2.12	11.3	0.821	292.4	49.9	0.085	2.20	0.998	0.046
Sr(II)	25°C	75.5	16.77	2.30	0.922	489.6	85.4	0.098	1.28	0.996	1.29
	35°C	84.6	17.54	2.23	0.930	544.7	97.9	0.089	1.24	0.995	2.09
	45°C	89.5	18.32	2.20	0.929	619.4	103.3	0.086	1.25	0.994	2.13

3.4. Reusability of microporous SiO2-TUF

The nanochannels' presence shortens the pathway of the ions toward the active sites on the adsorbent surface. It is essential for practical application to recycle the sorbent and efficiently use it again to remove more pollutants. For that purpose, we used HNO_3 solution as a stripping agent for Sr(II) and Cs(I) ions to regenerate SiO2-TUF. The HNO_3 solution concentration was selected as .02 and 0.05 M for Cs(I) and Sr(II), respectively. After the first regeneration cycle, SiO2-TUF removed 97% of the toxic ions compared to the freshly made adsorbent (Fig. 9). It is possible to regenerate SiO2-TUF for 8 cycles with an efficiency above 70%. However, in our work on stable ions of cesium and strontium, the SiO2-TUF regeneration in real radioactive samples should be contaminated with radioactive ions and should be removed as waste concentrate to be solidified.

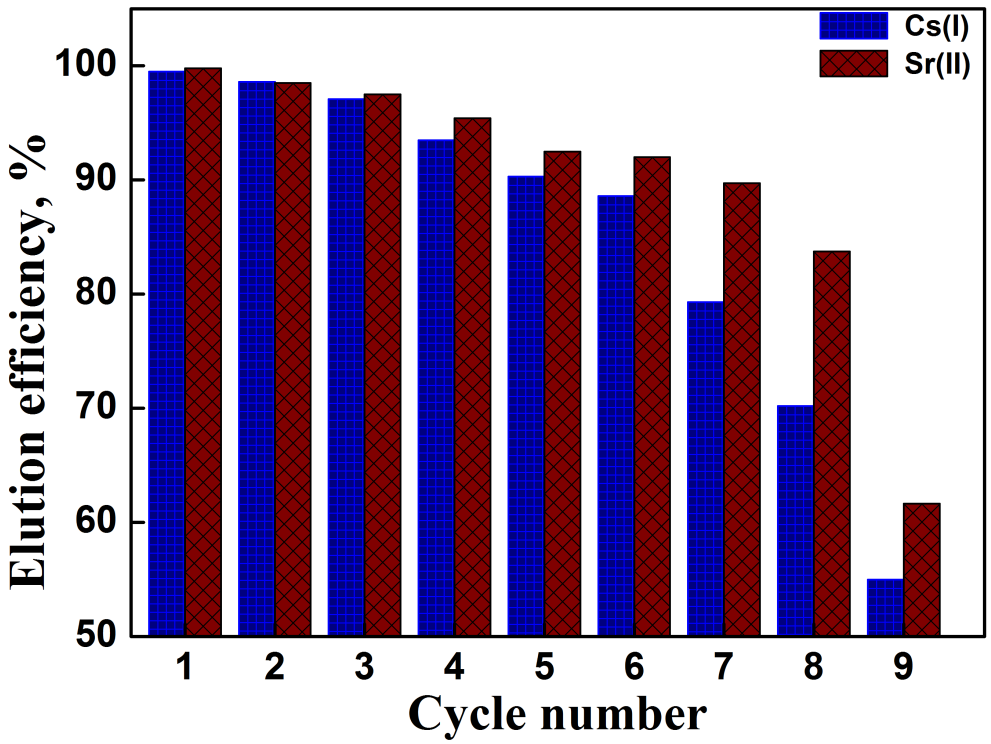

Figure 9: Effect of the recycling SiO2-TUF composite on the recovery of Sr(II) and Cs(I) ions over 8 cycles of sorption/desorption.

3.5. Adsorbent selectivity and ions removal from contaminated seawater

To prove the real applicability of SiO2-TUF on the removal of radioactive Sr(II) and Cs(I) from environmental samples, we used Mediterranean seawater samples as the carrying solution. The ions concentration in the seawater samples is summarized in Table 3. The Sr(II) concentration and Cs(I) in the seawater were chosen to be 1 mg/L, and the pH value was kept natural during the adsorption test. Even from such a complex system, the adsorption capacities of Sr(II) and Cs(I) using SiO2-TUF sorbent are 92.78 and 91.7%, respectively. This interesting finding suggests the usefulness of the designed SiO2-TUF for selective removal of radioactive Sr(II) and Cs(I) from the environmental seawater samples contains Rb(I) ions efficiently. The enhanced selectivity for Cs(I) and Sr(II) can be attributed to the additional Lewis acid-base interactions of the sulfur incorporated in SiO2-TUF with a soft acid (Cs(I) and Sr(II)) in the presence of competing ions such as Na(I), K(I), Ca(II), and Mg(II) which are harder than Cs(I) and Sr(II)

ions. This is a simple and easily scalable because sulfur a soft base, can partially donate an electron to soft acid a relatively soft Lewis acid compared with competing ions such as Na(I) and Mg(II) during the Cs(I) and Sr(II) ion-exchange; hard/soft acid/base (HSAB) theory which is a generalization of Lewis acid-base theory states that hard acids have high affinities for hard bases while soft acids exhibit high affinities for soft bases.[47]

Table 3. Adsorption of Cs(I) and Sr(II) ions from simultaneous seawater sample by 50 mg SiO2-TUF in 50 mL solution volume.

Ions conc. in seawater, mg/L	**Spiked sample, mg/L**		**Amount Adsorbed, mg/L**		**Adsorption Efficiency, %**	
Cs(I): 0.0172, Sr(II): 6.488, Na(I):12270.5, K(I): 421.8, Ca(II): 505.6, Mg(II): 1150, B(III): 3.95, Fe(III): 2.15, Cu(II):1.44, Ba: 69.9, Pb(II) 1.65, Cr(VI):17.08, Cd(II): 8.50, Mn(II):24.7, Ni(II): 62.7, U(VI): 0.0018, Cl^-: 22130, SO_4^{-2}: 2390, HCO_3^-: 129.5. Injected ions: Sr(II): 0.963, Cs(I): 0.9503, Rb(I):1.023	Cs(I)	Sr(II)	Cs(I)	Sr(II)	Cs(I)	Sr(II)
	0.9675	7.451	0.88	6.913	91.7	92.78

4. Conclusions

We introduced a microporous structure in which silica work as solid filler and thiourea/formaldehyde polymer particles filling the internal volume. The SiO2-TUF hybrid was prepared by a simple method based on the co-polymerization of the silica monolith with the thiourea/formaldehyde precursor. The produced composite provided a larger surface area (815.71 m^2/g) and micropores for easy adsorption of Cs(I) and Sr(II) from aqueous solutions. The adsorption process was enhanced by the thiol and amino groups on the surface of the composite, which offered active sites for the electrostatic interaction with the target ions. As a result, the composite exhibited maximum adsorption capacities of 40.3 and 75.5 mg g^{-1} at 25 °C for Cs(I)

and Sr(II), respectively. It was found that the solution pH has a vital role in determining the adsorption capacity and mechanism of both studied ions. The adsorption isotherm was best fitted by Sips model, and the pseudo-second-order rate equation best fits the uptake kinetics. The developed composite adsorbent's feasible application was further tested by removing Cs(I) and Sr(II) from seawater samples. The new adsorbent showed good selectivity towards the radioactive substances, despite the co-existence of ions with similar chemical nature in seawater. Furthermore, it was possible to regenerate SiO2-TUF by simple acid striping, giving a sorbent able to achieve 97% of the freshly made composite's adsorption capacity. Our research showed that the well-designed silica monolith/polymer composite could be used for the effective removal of radioactive material from seawater.

Reference

1. Zhang, X.; Gu, P.; Liu, Y., Decontamination of radioactive wastewater: State of the art and challenges forward. *Chemosphere* **2019,** *215*, 543-553.
2. El-Din, A. F. T.; Elshehy, E. A.; Abd El-Magied, M. O.; Atia, A. A.; El-Khouly, M. E., Decontamination of radioactive cesium ions using ordered mesoporous monetite. *RSC advances* **2018,** *8* (34), 19041-19050.
3. Zhang, X.; Liu, Y., Nanomaterials for radioactive wastewater decontamination. *Environmental Science: Nano* **2020,** *7* (4), 1008-1040.
4. El-Din, A. F. T.; El-Khouly, M. E.; Elshehy, E. A.; Atia, A. A.; El-Said, W. A., Cellulose acetate assisted synthesis of worm-shaped mesopores of MgP ion-exchanger for cesium ions removal from seawater. *Microporous and Mesoporous Materials* **2018,** *265*, 211-218.
5. Elshehy, E. A., Removal of uranium ions from liquid radioactive waste using modified aluminosilica. *Separation Science and Technology* **2017,** *52* (11), 1852-1861.
6. Awual, M. R.; Yaita, T.; Taguchi, T.; Shiwaku, H.; Suzuki, S.; Okamoto, Y., Selective cesium removal from radioactive liquid waste by crown ether immobilized new class conjugate adsorbent. *Journal of hazardous materials* **2014,** *278*, 227-235.
7. Yang, H.-M.; Park, C. W.; Kim, I.; Yoon, I.-H.; Sihn, Y., Sulfur-modified chabazite as a low-cost ion exchanger for the highly selective and simultaneous removal of cesium and strontium. *Applied Surface Science 536*, 147776.
8. El-Din, A. F. T.; Elshehy, E. A.; El-Khouly, M. E., Cellulose acetate/EDTA-chelator assisted synthesis of ordered mesoporous HAp microspheres for efficient removal of radioactive species from seawater. *Journal of environmental chemical engineering* **2018,** *6* (5), 5845-5854.
9. Ali, F.; Elshehy, E. A.; Mohamed, E., Cellulose Acetate/EDTA-Chelator Assisted Synthesis of. *J. Environ. Radioact* **2017,** *178* (179), 290-296.
10. Tonoike, K.; Sono, H.; Umeda, M.; Yamane, Y.; Kugo, T.; Suyama, K.; Nakajima, K., Nuclear Back-end and Transmutation Technoogy for Waste Disposal. Chapter: 2015.
11. Mohapatra, P.; Bhattacharyya, A.; Manchanda, V., Selective separation of radio-cesium from acidic solutions using supported liquid membrane containing chlorinated cobalt dicarbollide (CCD) in phenyltrifluoromethyl sulphone (PTMS). *Journal of hazardous materials* **2010,** *181* (1-3), 679-685.

12. Chen, R.; Tanaka, H.; Kawamoto, T.; Asai, M.; Fukushima, C.; Na, H.; Kurihara, M.; Watanabe, M.; Arisaka, M.; Nankawa, T., Selective removal of cesium ions from wastewater using copper hexacyanoferrate nanofilms in an electrochemical system. *Electrochimica acta* **2013,** *87*, 119-125.
13. Rahman, R. A.; Moamen, O. A.; Abdelmonem, N.; Ismail, I., Optimizing the removal of strontium and cesium ions from binary solutions on magnetic nano-zeolite using response surface methodology (RSM) and artificial neural network (ANN). *Environmental research* **2019,** *173*, 397-410.
14. Xing, M.; Zhuang, S.; Wang, J., Adsorptive removal of strontium ions from aqueous solution by graphene oxide. *Environmental Science and Pollution Research* **2019,** *26* (29), 29669-29678.
15. Choi, J.-W.; Park, Y.-J.; Choi, S.-J., Synthesis of Metal–Organic Framework ZnO x-MOF@ MnO2 Composites for Selective Removal of Strontium Ions from Aqueous Solutions. *ACS omega* **2020,** *5* (15), 8721-8729.
16. Ali, S.; Shah, I. A.; Huang, H., Selectivity of Ar/O2 plasma-treated carbon nanotube membranes for Sr (II) and Cs (I) in water and wastewater: Fit-for-purpose water treatment. *Separation and Purification Technology* **2020,** *237*, 116352.
17. Prajitno, M. Y.; Tangparitkul, S.; Zhang, H.; Harbottle, D.; Hunter, T. N., The effect of cationic surfactants on improving natural clinoptilolite for the flotation of cesium. *Journal of Hazardous Materials* **2020,** *402*, 123567.
18. Milyutin, V.; Nekrasova, N.; Yanicheva, N. Y.; Kalashnikova, G.; Ganicheva, Y. Y., Sorption of cesium and strontium radionuclides onto crystalline alkali metal titanosilicates. *Radiochemistry* **2017,** *59* (1), 65-69.
19. Yang, H.-M.; Park, C. W.; Kim, I.; Yoon, I.-H., Hollow flower-like titanium ferrocyanide structure for the highly efficient removal of radioactive cesium from water. *Chemical Engineering Journal* **2020,** *392*, 123713.
20. Balazs, A. C.; Emrick, T.; Russell, T. P., Nanoparticle polymer composites: where two small worlds meet. *Science* **2006,** *314* (5802), 1107-1110.
21. Caseri, W., Nanocomposites of polymers and inorganic particles: preparation, structure and properties. *Materials Science and Technology* **2006,** *22* (7), 807-817.
22. Schadler, L.; Brinson, L. C.; Sawyer, W., Polymer nanocomposites: a small part of the story. *Jom* **2007,** *59* (3), 53-60.
23. Hajji, P.; David, L.; Gerard, J.; Pascault, J.; Vigier, G., Synthesis, structure, and morphology of polymer–silica hybrid nanocomposites based on hydroxyethyl methacrylate. *Journal of Polymer Science Part B: Polymer Physics* **1999,** *37* (22), 3172-3187.
24. Althues, H.; Henle, J.; Kaskel, S., Functional inorganic nanofillers for transparent polymers. *Chemical Society Reviews* **2007,** *36* (9), 1454-1465.
25. Jordan, J.; Jacob, K. I.; Tannenbaum, R.; Sharaf, M. A.; Jasiuk, I., Experimental trends in polymer nanocomposites—a review. *Materials science and engineering: A* **2005,** *393* (1-2), 1-11.
26. El-Said, W. A.; El-Khouly, M. E.; Ali, M. H.; Rashad, R. T.; Elshehy, E. A.; Al-Bogami, A. S., Synthesis of mesoporous silica-polymer composite for the chloridazon pesticide removal from aqueous media. *Journal of Environmental Chemical Engineering* **2018,** *6* (2), 2214-2221.
27. Hussein, M. A.; Alamry, K. A.; El Shishtawy, R. M.; Elshehy, E. A.; El-Said, W. A., Nanoporous colorant sensors and captors for simultaneous recognition and recovery of gold from E-wastes. *Waste Management* **2020,** *116*, 166-178.
28. El-Safty, S. A.; Shenashen, M. A.; Sakai, M.; Elshehy, E.; Halada, K., Detection and recovery of palladium, gold and cobalt metals from the urban mine using novel sensors/adsorbents designated with nanoscale wagon-wheel-shaped pores. *JoVE (Journal of Visualized Experiments)* **2015,** (106), e53044.
29. Elshehy, E. A.; Shenashen, M. A.; Abd El-Magied, M. O.; Tolan, D. A.; El-Nahas, A. M.; Halada, K.; Atia, A. A.; El-Safty, S. A., Selective Recovery of Silver (I) Ions from E-Waste using Cubically Multithiolated Cage Mesoporous Monoliths. *European Journal of Inorganic Chemistry* **2017,** *2017* (41), 4823-4833.
29. Timina A.; Rumyantseva E.,; Laninb S.N.; Rychkovab S.A.; Guseynovc S.S.; Solomonova A.V.; Antina E.V., Preparation and surface properties of mesoporous silica particles modified with poly(N-vinyl-

2-pyrrolidone) as a potential adsorbent for bilirubin removal, *Materials Chemistry and Physics*, **2014**, *xxx*, 1-11.
30. Zhi K.; Wang L.; Zhang Y.; Jiang Y.; Zhang L.; Yasin A.;, Influence of Size and Shape of Silica Supports on the Sol¯Gel Surface Molecularly Imprinted Polymers for Selective Adsorption of Gossypol. *Materials (Basel)*. **2018**, *11*(5), 777.
32. Zhu, Y.; Liu, Y.; Ge, Z.; Zhang, Y.; Li, M.; Wei, S., Improved thermal stability of melamine resin spheres and electrochemical properties of their carbon derivatives induced by F127. *Journal of Materials Science* **2020**, *55*, 12114–12126.
33. Donia, A.; Atia, A.; Daher, A.; Desouky, O.; Elshehy, E., Synthesis of amine/thiol magnetic resin and study of its interaction with Zr (IV) and Hf (IV) ions in their aqueous solutions. *Journal of dispersion science and technology* **2011,** *32* (5), 634-641.
34. Chang, C.; Yang, X.; Xiang, S.; Que, H.; Li, M., Thiourea aldehyde resin-based carbon/graphene composites for high-performance supercapacitors. *Journal of Solid State Electrochemistry* **2018,** *22* (1), 113-121.
35. Brunetti, V.; Blum, B.; Salvarezza, R.; Arvia, A.; Schilardi, P.; Cuesta, A.; Gayone, J.; Zampieri, G., Scanning Tunneling Microscopy, Fourier Transform Infrared Reflection− Absorption Spectroscopy, and X-ray Photoelectron Spectroscopy of Thiourea Adsorption from Aqueous Solutions on Silver (111). *The Journal of Physical Chemistry B* **2002,** *106* (38), 9831-9838.
36. Fu, L.; Zhang, L.; Wang, S.; Peng, J.; Zhang, G., Selective adsorption of Ag^{+} by silica nanoparticles modified with 3-Amino-5-mercapto-1, 2, 4-triazole from aqueous solutions. *Journal of Molecular Liquids* **2017,** *241*, 292-300.
37. Hasan, S.; Iasir, A. R. M.; Ghosh, T. K.; Sen Gupta, B.; Prelas, M. A. In *Characterization and Adsorption Behavior of Strontium from Aqueous Solutions onto Chitosan-Fuller's Earth Beads*, Healthcare, Multidisciplinary Digital Publishing Institute: 2019; p 52.
38. Ho, Y.-S., Review of second-order models for adsorption systems. *Journal of hazardous materials* **2006,** *136* (3), 681-689.
39. Weber, W. J.; Morris, J. C., Equilibria and capacities for adsorption on carbon. *Journal of the Sanitary Engineering Division* **1964,** *90* (3), 79-108.
40. Kumar E; Bhatnagar A; Ji M; Jung W; Lee S H; Kim S J; Lee G; Song H; Choi J Y; Yang J S; Jeon B H, Defluoridation from aqueous solutions by granular ferric hydroxide (GFH) Water Res., **2008**, *43*(2), 490-498.
41. Gupta V K; Ali I ; Saini V K, Defluoridation of wastewaters using waste carbon slurry, Water Res., **2007**, *41*, 3307-3316.
42. Freundlich, H., Über die adsorption in lösungen. *Zeitschrift für physikalische Chemie* **1907,** *57* (1), 385-470.
43. Belhachemi, M.; Addoun, F., Comparative adsorption isotherms and modeling of methylene blue onto activated carbons. *Applied water science* **2011,** *1* (3-4), 111-117.
44. Günay, A.; Arslankaya, E.; Tosun, I., Lead removal from aqueous solution by natural and pretreated clinoptilolite: adsorption equilibrium and kinetics. *Journal of hazardous materials* **2007,** *146* (1-2), 362-371.
45. Allen, S.; Mckay, G.; Porter, J. F., Adsorption isotherm models for basic dye adsorption by peat in single and binary component systems. *Journal of colloid and interface science* **2004,** *280* (2), 322-333.

46. Hoa, Y-S.; Chiu W-T.; Wang C-C., Regression analysis for the sorption isotherms of basic dyeson sugarcane dust. BioresourceTechnology **2005**, *96*, 1285–1291.

47. H-M. Yang, C. W. Park, I. Kim, I-H. Yoon, Y. Sihn, Sulfur-modified chabazite as a low-cost ion exchanger for the highly selective and simultaneous removal of cesium and strontium, Applied Surface Science 536 (2021) 147776.

608